# Two-stage Optimization for Active Distribution Systems Based on Operating Ranges of Soft Open Points and Energy Storage System

Can Wang, Jianjun Sun, Meng Huang, Xiaoming Zha, and Wei Hu

*Abstract*—**Due to the lack of flexible interconnection devices, power imbalances between networks cannot be relieved effectively. Meanwhile, increasing the penetration of distributed generators exacerbates the temporal power imbalances caused by large peak-valley load differences. To improve the operational economy lowered by spatiotemporal power imbalances, this paper proposes a two-stage optimization strategy for active distribution networks (ADNs) interconnected by soft open points (SOPs). The SOPs and energy storage system (ESS) are adopted to transfer power spatially and temporally, respectively. In the day-ahead scheduling stage, massive stochastic scenarios against the uncertainty of wind turbine output are generated first. To improve computational efficiency in massive stochastic scenarios, an equivalent model between networks considering sensitivities of node power to node voltage and branch current is established. The introduction of sensitivities prevents violations of voltage and current. Then, the operating ranges (ORs) of the active power of SOPs and the state of charge (SOC) of ESS are obtained from models between networks and within the networks, respectively. In the intraday corrective control stage, based on day-ahead ORs, a receding-horizon model that minimizes the purchase cost of electricity and voltage deviations is established hour by hour. Case studies on two modified ADNs show that the proposed strategy achieves spatiotemporal power balance with lower cost compared with traditional strategies.**

*Index Terms*—**Active distribution system, operating range, sensitivity, soft open point (SOP), power imbalance.**

## Nomenclature

### A. Sets

| | |
|---|---|
| $\Omega_{\text{sen}}^{\text{sto}}$ | Set of stochastic scenarios |
| $\Omega_{\text{sen}}^{\text{typ}}$ | Set of typical scenarios |
| $\Psi_{\text{nd}}^{m}$ | Set of nodes in network $m$ |
| $\Psi_{\text{nd}}^{\text{SOP}}$ | Set of nodes that connect to soft open points (SOPs) |
| $\Phi_{\text{br}}$ | Set of branches |
| $\Phi_{\text{br}}^{m}$ | Set of branches in network $m$ |
| $\Theta_{c}^{\text{up}}$ | Set of purchased active power pairs |
| $\Xi_{k}^{\varepsilon}$ | Set of scenarios whose forecast error belongs to the $k^{\text{th}}$ forecast error interval |

### B. Parameters

| | |
|---|---|
| $\alpha_{\text{up}}$, $\alpha_{\text{vd}}$ | Objective weights of total purchase cost and voltage deviation |
| $\varepsilon$ | Forecast error |
| $\varepsilon_{\min}$, $\varepsilon_{\max}$ | The minimum and maximum forecast errors |
| $\varepsilon_{s}$ | Small interval of forecast error |
| $\varepsilon_{k}$ | Forecast error of the $k^{\text{th}}$ forecast error interval |
| $\eta_{i}^{\text{ch}}$, $\eta_{i}^{\text{dis}}$ | Charging and discharging efficiencies of energy storage system (ESS) at node $i$ |
| $\Delta_{\max}^{\text{SCB}}$ | The maximum switch times of shunt capacitor bank (SCB) |
| $\Delta\boldsymbol{P}_{t,\omega}$, $\Delta\boldsymbol{Q}_{t,\omega}$ | Vectors of difference of node active and reactive power during period $t$ in scenario $\omega$ |
| $\Delta\boldsymbol{\theta}_{t,\omega}$, $\Delta\boldsymbol{U}_{t,\omega}$ | Vectors of difference of voltage phase and magnitude during period $t$ in scenario $\omega$ |
| $\boldsymbol{\delta}_{t,\omega}^{IP}$, $\boldsymbol{\delta}_{t,\omega}^{IQ}$ | Matrices of sensitivity of branch current with respect to node active power and reactive power |
| $A_{i}^{\text{SOP}}$ | Loss coefficient of SOP at node $i$ |
| $c_{t}^{\text{pur}}$ | Unit purchase cost of electricity during period $t$ |
| $E_{i,\text{ini},\omega}$, $E_{i,T,\omega}$ | Initial state of charge (SOC) and final SOC of ESS at node $i$ in scenario $\omega$ |
| $E_{\min}$, $E_{\max}$ | The minimum and maximum values of SOC |
| $E_{\min}^{i,t,k}$, $E_{\max}^{i,t,k}$ | The minimum and maximum values of SOC of ESS at node $i$ during period $t$ in the $k^{\text{th}}$ forecast error interval |
| $f_{m}^{\text{up}}$, $f_{m}^{\text{vd}}$ | Total purchase cost and voltage deviations before optimization in network $m$ |
| $i_{ij,\max}$ | The maximum square of current of branch $ij$ |
| $\boldsymbol{I}_{t,\omega}^{0}$, $\boldsymbol{I}_{t,\omega}'$ | Vectors of branch current before and after optimization during period $t$ in scenario $\omega$ |

Manuscript received: May 24, 2022; revised: August 9, 2022; accepted: September 5, 2022. Date of CrossCheck: September 5, 2022. Date of online publication: October 19, 2022.

This work was supported by the Science and Technology Project of State Grid Corporation of China (No. 5400-202199281A-0-0-00).



C. Wang, J. Sun (corresponding author), M. Huang, and X. Zha are with the School of Electrical Engineering and Automation, Wuhan University, Wuhan 430072, China (e-mail: wangcanee@whu. edu. cn; jjsun@whu. edu. cn; meng. huang@whu.edu.cn; xmzha@whu.edu.cn).

W. Hu is with the State Grid Hubei Electric Power Corporation, Wuhan 430070, China (e-mail: dmqhw2004@163.com).

DOI: 10.35833/MPCE.2022.000303

| | |
|---|---|
| $\boldsymbol{J}_{t,\omega}^{P\theta}$, $\boldsymbol{J}_{t,\omega}^{PU}$, $\boldsymbol{J}_{t,\omega}^{Q\theta}$, $\boldsymbol{J}_{t,\omega}^{QU}$ | Submatrices of Jacobian matrix during period $t$ in scenario $\omega$ |
| $\boldsymbol{J}$ | Jacobian matrix |
| $N$ | Number of networks |
| $N^{\mathrm{S}}$ | Number of scenarios |
| $N^{\mathrm{E}}$ | Number of error intervals |
| $N_{\max}^{\mathrm{SCB}}$ | The maximum number of banks switched in once |
| $p_{\omega}$ | Probability of scenario $\omega$ from $\Omega_{\mathrm{sen}}^{\mathrm{typ}}$ |
| $P^{\mathrm{link}}$ | Global value of active power of SOP |
| $P_{l+1}^{\mathrm{link}}$ | Global value after $l+1$ iterations |
| $P_{i,\max}^{\mathrm{ch}}$, $P_{i,\max}^{\mathrm{dis}}$ | The maximum charging and discharging power of ESS at node $i$ |
| $P_{i,t,k,\min}^{\mathrm{SOP}}$, $P_{i,t,k,\max}^{\mathrm{SOP}}$ | The minimum and maximum values of active power of SOP at node $i$ during period $t$ in the $k^{\mathrm{th}}$ forecast error interval |
| $q^{\mathrm{SCB}}$ | Unit reactive capacity of SCB |
| $Q_{i,\min}^{\mathrm{SVC}}$, $Q_{i,\max}^{\mathrm{SVC}}$ | The minimum and maximum reactive power of SVC at node $i$ |
| $r_{ij}$, $x_{ij}$ | Resistance and reactance of branch $ij$ |
| $r_{ij,m}$ | Resistance of branch $ij$ in network $m$ |
| $S_i^{\mathrm{SOP}}$ | Capacity of SOP at node $i$ |
| $S_i^{\mathrm{ESS}}$ | Capacity of ESS at node $i$ |
| $T$ | Number of periods |
| $u_{i,\min}$, $u_{i,\max}$ | The minimum and maximum squares of voltage magnitude at node $i$ |
| $\boldsymbol{U}_{t,\omega}^{0}$, $\boldsymbol{U}_{t,\omega}'$ | Vectors of voltage magnitude before and after optimization during period $t$ in scenario $\omega$ |
| $w_1^{l+1}$, $s_1^{l+1}$ | Raw residual and dual residual of network 1 after $l+1$ iterations |

*C. Variables*

| | |
|---|---|
| $\alpha_{m,c,\omega}$ | Weight of the $c^{\mathrm{th}}$ pair of purchased active power in scenario $\omega$ in network $m$ |
| $\gamma_{i,t,\omega}^{\mathrm{ch}}$, $\gamma_{i,t,\omega}^{\mathrm{dis}}$ | 0-1 indexes indicating whether ESS at node $i$ charges or discharges during period $t$ in scenario $\omega$ |
| $\theta_{k,t,\omega}$ | Voltage phase of node $k$ during period $t$ in scenario $\omega$ |
| $\theta_{ij,t,\omega}$ | Voltage phase deviation between node $i$ and node $j$ during period $t$ in scenario $\omega$ |
| $\Delta P_{m,\omega,t_c^1,t_c^2}^{\mathrm{up}}$ | Substituted variable for the absolute value between $P_{m,t_c^1,\omega}^{\mathrm{up}}$ and $P_{m,t_c^2,\omega}^{\mathrm{up}}$ |
| $E_{i,t,k}$ | SOC of ESS at node $i$ during period $t$ in the $k^{\mathrm{th}}$ forecast error interval |
| $E_{i,t,\omega}$ | SOC of ESS at node $i$ during period $t$ in scenario $\omega$ |
| $E_{i,t}$ | SOC of ESS at node $i$ during period $t$ |
| $i_{m,ij,t,\omega}$ | Square of current of branch $ij$ in period $t$ in scenario $\omega$ in network $m$ |
| $i_{ij,t,\omega}$ | Square of current of branch $ij$ during period $t$ in scenario $\omega$ |
| $I_{ij,t,\omega}$ | Current of branch $ij$ during period $t$ in scenario $\omega$ |
| $\boldsymbol{M}_{t,\omega}^{I\theta}$, $\boldsymbol{M}_{t,\omega}^{IU}$ | Matrices consisting of $\partial I_{ij,t,\omega}/\partial P_{k,t,\omega}$ and $\partial I_{ij,t,\omega}/\partial Q_{k,t,\omega}$ |
| $N_{i,t}^{\mathrm{SCB}}$ | Number of banks of SCB switched in at node $i$ during period $t$ |
| $P_{m,t,\omega}^{\mathrm{nl}}$ | Net active load in network $m$ during period $t$ in scenario $\omega$ |
| $P_{m,t,\omega}^{\mathrm{SOP}}$ | Active power of SOP connected to network $m$ during period $t$ in scenario $\omega$ |
| $P_{i,t}^{\mathrm{SCB}}$ | Reactive power of SCB at node $i$ during period $t$ |
| $P_{ij,t,\omega}$, $Q_{ij,t,\omega}$ | Active and reactive power of branch $ij$ during period $t$ in scenario $\omega$ |
| $P_{i,t,\omega}$, $Q_{i,t,\omega}$ | Injected active and reactive power of node $i$ during period $t$ in scenario $\omega$ |
| $P_{i,t,\omega}^{\mathrm{SOP}}$, $Q_{i,t,\omega}^{\mathrm{SOP}}$ | Active and reactive power of SOP at node $i$ during period $t$ in scenario $\omega$ |
| $P_{i,t,\omega}^{\mathrm{ch}}$, $P_{i,t,\omega}^{\mathrm{dis}}$ | Charging and discharging active power of ESS at node $i$ during period $t$ in scenario $\omega$ |
| $P_{m,t,\omega}^{\mathrm{up}}$ | Purchased active power during period $t$ in network $m$ in scenario $\omega$ |
| $P_{m,t}^{\mathrm{up}}$ | Purchased active power during period $t$ in network $m$ |
| $P_{i,t,\omega}^{\mathrm{SOP,L}}$ | Active power loss of SOP at node $i$ during period $t$ in scenario $\omega$ |
| $P_{i,t,\omega}^{\mathrm{SVC}}$ | Reactive power of series var compensator (SVC) at node $i$ during period $t$ in scenario $\omega$ |
| $P_{i,t}^{\mathrm{SOP}}$, $P_{i,t}^{\mathrm{SOP,L}}$ | Active power and active power losses of SOP at node $i$ during period $t$ |
| $u_{i,m,t}'$ | Substituted variable for the absolute value between 1 and the square of voltage magnitude of node $i$ during period in network $m$ |
| $u_{i,t,\omega}$ | Square of voltage of node $i$ during period $t$ in scenario $\omega$ |
| $U_{i,t,\omega}$ | Voltage of node $i$ during period $t$ in scenario $\omega$ |

## I. INTRODUCTION

WITH the higher penetration of wind turbines (WTs) and other distributed generators (DGs) [1], uncertainties in their outputs exacerbate power imbalances between different networks in the space dimension and expand peak-valley differences in net load within a network in the time dimension [2]. Under this context, soft open points (SOPs) [3], which can transfer active power between networks and compensate reactive power spatially, and energy storage systems (ESSs) [4], which can shift peak power to valley power temporally, have been widely studied. Combined with other regulatory devices, better system operation states can be achieved in active distribution networks (ADNs) [5].

SOPs were originally proposed in [3] and consist of voltage source converters (VSCs) connected by capacitors. A simulation case composed of three IEEE standard networks was analyzed in [5], where a five-terminal SOP worked as an energy hub that transferred active power between networks. To cope with the complex uncertainties imposed by photovoltaic generations, a real-time scheduling method with SOPs via a multi-timescale framework was proposed in [6], where SOPs were coordinated with on-load tap changer (OLTC), shunt capacitor bank (SCB), and series voltage regulator (SVR). A two-stage robust model was established in [7] to address the uncertainties of photovoltaic outputs, where SOPs were adopted to eliminate voltage violations and reduce the power losses. For a three-phase unbalanced condition in an ADN, an SOP-based operation strategy was proposed in [8], where power losses were reduced and the three-phase unbalance was mitigated. A data-driven operation strategy of SOP was proposed in [9] with inaccurate parameters and frequent changes of operation states, where multiple SOPs were used to connect different areas inside a single ADN. SOPs integrated with ESS were proposed in [10] to improve the flexibility in ADNs, where losses of SOP with energy storage were modeled considering its subsystems. In addition, two IEEE 33-node networks were connected via a SOP with ESS in [10]. Considering the flexible interconnection and multiple application conditions introduced by SOPs, balancing power between different ADNs with the active power transfer of SOPs is another application scope.

To assess the power imbalance condition [11] and other existing problems in ADNs [5], the coordination of multiple regulatory devices has been studied. To mitigate the imbalance condition of feeder loads, an enhanced SOCP-based method via a multiterminal SOP was proposed in [11]. In addition, SOPs were also applied in the load balance of different feeders in an ADN in [12], which performed better than the network reconfiguration. Aiming at the power flow fluctuation and load imbalance condition caused by the large-scale integration of DGs, a multiterminal SOP was coordinated in [13] with DGs, OLTC, and controllable loads, where the SOP flexibly connected feeders in the distribution network. In sum, SOPs together with other devices are able to balance power spatially and temporally.

Optimization results from the day-ahead stage can provide promising references for the intraday stage with the coordination of the day-ahead stage and the intraday stage. Based on day-ahead load forecast data, the hourly reactive power of DGs was determined in [12] in coordination with switching operations of OLTC and SCBs. Differences between actual and forecast load data were assumed to be small in [12], the strategy of which lacked reference for the intraday stage. A multi-timescale framework for volt/var optimization was proposed in [13], which coordinated the tap changer on a slow timescale (hourly basis) and the ESS on a fast timescale (15-min basis). The ESS power setpoints obtained in the first stage had no connection to the results in the second stage. The operation curve for the state of charge (SOC) of ESS was predetermined in a day-ahead model in [14], which was unchangeable in the intraday dispatch stage. Since the intraday hourly forecast data may differ greatly from day-ahead data, the intraday rescheduling of an ESS based on day-ahead schemes should be studied. Moreover, in the day-ahead stage, optimization results of SOPs that may provide beneficial references for intraday corrective control are always omitted [14]. An ESS in the intraday stage was dispatched hourly within the optimized SOC limits obtained from the day-ahead stage in [15], where the limits worked as operating ranges (ORs) for the ESS. Therefore, two stages should be coordinated optimally, where the optimal decisions of the intraday stage should be based on the day-ahead schedule.

To cope with the uncertainties of loads and outputs of DGs, robust optimization and stochastic optimization have been widely studied. To ensure the robustness of dispatch decisions under the uncertainties of DGs, a distributionally robust real-time power dispatch model for a coupled transmission grid and ADNs was proposed in [16]. The proposed stochastic framework in [17] considered the uncertainties of DGs, which were converted to deterministic problems with probabilities. A stochastic model was established to minimize power losses and avoid voltage violations in [18], taking load forecast errors into account. Nevertheless, stochastic programming relies heavily on the accurate formulation of the probability density function, which may be difficult to obtain, while conservativeness can only be reduced but not eliminated in the robust model.

The alternating direction multiplier method (ADMM) is a promising distributed method that can be applied to the optimization of power systems [19]. For a large-scale ADN with a given division of areas, an ADMM was used to carry out a distributed reactive optimization in [20]. For large numbers of scenarios, it will take the method like the ADMM more time to complete the whole optimization if specific power flow constraints such as DistFlow constraints are included in the model. In this context, a sensitivity-based method can accelerate the computation but with a loss of accuracy. A straightforward analytical derivation of node voltage and line current sensitivities was provided in [21] based on the sparse compound matrix $\boldsymbol{Y}$. The sensitivities of node voltages with respect to the OLTC were calculated to estimate the voltage in [22]. Similarly, an efficient sensitivity calculation method was used in [23] to update the voltage sensitivities online with respect to the settings of discrete-acting devices. Consequently, to improve the computational efficiency of optimal power flow in massive scenarios, the sensitivity-based optimization method can be adopted.

Motivated by the above facts, to work against spatial power imbalances between networks and temporal power imbalances inside a network and offer a flexible intraday regulation strategy for SOPs and ESSs, this paper focuses on presenting an optimization strategy for flexibly interconnected ADNs under WT uncertainty, including the day-ahead scheduling and intraday corrective control stages. The main contributions of this paper are summarized as follows.

1) To address the limitations of the day-ahead scheduling stage, which provides reference curves for the intraday corrective control stage, ORs of active power of SOPs and the

SOC of ESS are constructed from optimization results of large numbers of stochastic scenarios generated by WT uncertainty, of which the total cost is less than that of fixed operation curves in ADNs.

2) To improve the computational efficiency of ORs obtained from the results in large numbers of stochastic scenarios, each network-connected SOP is equivalent to an entity with net loads. Then, current and voltage sensitivities with respect to node power to prevent violations are considered rather than specific power flow constraints, which guarantees the effectiveness of ORs.

The rest of this paper is organized as follows. Section II outlines the framework of spatiotemporal power balance. Sections III and IV formulate the power balancing models in the day-ahead scheduling stage and intraday corrective control stage, respectively. Section V provides the implementation algorithm. Section VI presents the numerical results and an analysis of two modified flexibly interconnected ADNs. Finally, Section VII concludes the paper.

## II. Framework of Spatiotemporal Power Balance

### A. Flexibly Interconnected ADNs

A flexible network consisting of multiple ADNs interconnected by SOPs has been studied in this paper. An example is shown in Fig. 1, where a two-terminal SOP connects two IEEE 33-node ADNs. ESS is applied to regulate active power while SCBs and static var compensator (SVC) are applied to regulate reactive power within network.

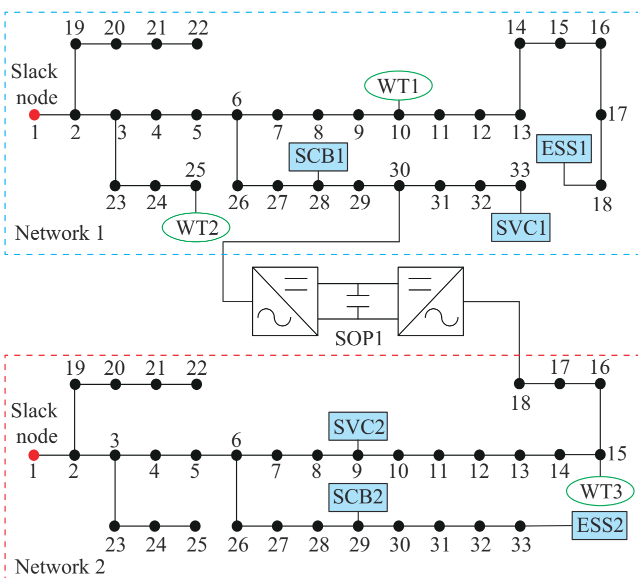


Fig. 1. Two IEEE 33-node ADNs connected by a two-terminal SOP.

### B. Coordination of Two Stages

A two-stage optimization strategy for spatiotemporal power balancing in flexibly interconnected ADNs is proposed in this paper. The timescales for the two stages are 24 hours and 1 hour, respectively. The framework of the proposed strategy is shown in Fig. 2, where $x_1$ is the purchase cost of electricity; $x_2$ is the voltage deviation; $x_3$ is the computing time; and $x_4$ is the voltage or current violation.

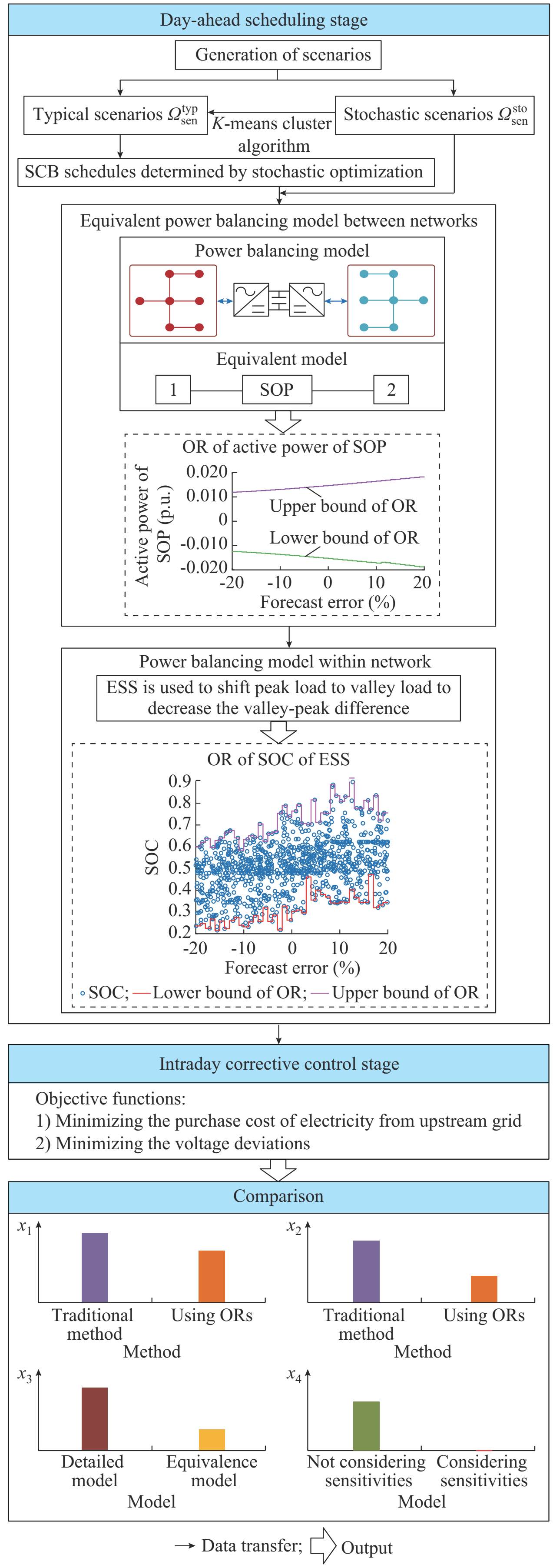


Fig. 2. Framework of proposed strategy.

Different from continuous-acting devices such as SOPs and ESSs, SCBs are discrete-acting devices. SCB schedules are generated through stochastic optimization.

First, large numbers of stochastic scenarios are generated through the Monte Carlo method according to the day-ahead forecast error of WT power, denoted as $\Omega_{\text{sen}}^{\text{sto}}$. Then, the $K$-means cluster algorithm is adopted to generate several typical scenarios, denoted as $\Omega_{\text{sen}}^{\text{typ}}$. Finally, SCB schedules are obtained through stochastic optimization based on typical scenarios. In addition, the SCB schedules will not be changed in the intraday corrective control stage.

In the day-ahead scheduling model between networks, each ADN is equivalent to an entity only with net active and reactive loads to improve computation efficiency in massive scenarios. Meanwhile, sensitivities are introduced to prevent violations of voltage and current in ADNs with the integration of an SOP instead of specific power flow constraints. Since active power can be transferred through the SOP, the SOP is applied to balance power spatially. In the day-ahead scheduling stage, with the objective of minimizing the sum of the purchased active power in 24 hours from all networks, the optimal active power of SOP in each scenario is obtained.

For the generation of OR, the forecast error range is divided equally into several error intervals considering WT uncertainty first. Then, considering $\Omega_{\text{sen}}^{\text{sto}}$, power flow optimization is carried out in each scenario. Based on the optimization results, the upper and lower limits of the active power of SOP and the SOC of ESS are chosen as the OR in each error interval. The whole OR consists of the ORs in all error intervals. To apply ORs in the intraday stage, the error interval in which the forecast error of WT power is located is determined first. Then, the OR in this interval is selected as the OR for the active power of SOP and the SOC of ESS.

In the day-ahead scheduling model within a single network, considering detailed power flow constraints, the power of the ESS and SVC is optimized with the objective of minimizing the weighted sum of peak-valley differences of purchased active power based on the optimal active power of the SOP. Similarly, ORs of the SOC of ESS can be constructed. Because the purchase cost of electricity is the main focus of the power balance and the reactive power has little effect on it, the reactive power of the SVC is omitted in the day-ahead scheduling stage.

In the intraday corrective control stage, the optimization model is established and solved by the ADMM hourly. First, specific ORs of the SOP and ESS should be determined based on hourly forecast errors compared with day-ahead forecast data. Then, with the objective of minimizing the weighted sum of the purchase cost of electricity and voltage deviations, the active power of SOP and the SOC of ESS are optimized in determined ORs, while the reactive power of SOP and SVC is regulated within capacity. Finally, according to the optimization results, the power of the SOP, ESS, and SVC is adjusted hourly by the distribution network operator.

The final optimization results indicate that the proposed strategy using ORs performs better than the traditional strategy. Meanwhile, it takes the equivalent model less time than the detailed model to complete optimization in massive scenarios. In addition, voltage or current violations never occur in the equivalent model when considering sensitivities. By comparison, voltage violations occur in the equivalent model without considering sensitivities.

## III. Power Balancing Model in Day-ahead Scheduling Stage

### *A. Determination of Schedule for Discrete-acting Devices*

#### *1) Objective Function*

The model to determine the schedule for discrete-acting devices such as SCB minimizes the weighted total purchase cost of electricity from the upstream grid in all typical scenarios $\Omega_{\text{sen}}^{\text{typ}}$.

$$\text{(P0)}\ \min f^{\text{da}} = p_\omega \sum_{m=1}^{N}\sum_{t=1}^{T} c_t^{\text{pur}} P_{m,t,\omega}^{\text{up}} \quad \omega \in \Omega_{\text{sen}}^{\text{typ}} \tag{1}$$

#### *2) Power Flow Constraints*

The DistFlow model is adopted to model the power flow in the ADN. The mathematical formulations can be described as:

$$\begin{cases} \sum\limits_{ik \in \Phi_{\text{br}}} P_{ik,t,\omega} - \left(P_{ji,t,\omega} - r_{ji} i_{ji,t,\omega}\right) = P_{i,t,\omega} \\ \sum\limits_{ik \in \Phi_{\text{br}}} Q_{ik,t,\omega} - \left(Q_{ji,t,\omega} - x_{ji} i_{ji,t,\omega}\right) = Q_{i,t,\omega} \\ P_{i,t,\omega} = \left(P_{i,t,\omega}^{\text{WT}} + P_{i,t,\omega}^{\text{SOP}} + P_{i,t,\omega}^{\text{dis}} - P_{i,t,\omega}^{\text{ch}}\right) - P_{i,t,\omega}^{\text{ld}} \\ Q_{i,t,\omega} = Q_{i,t}^{\text{SCB}} + Q_{i,t,\omega}^{\text{SVC}} + Q_{i,t,\omega}^{\text{SOP}} - Q_{i,t,\omega}^{\text{ld}} \\ u_{i,t,\omega} - u_{j,t,\omega} + \left(r_{ij}^2 + x_{ij}^2\right) i_{ij,t,\omega} = 2\left(r_{ij} P_{ij,t,\omega} + x_{ij} Q_{ij,t,\omega}\right) \\ i_{ij,t,\omega} u_{i,t,\omega} = P_{ij,t,\omega}^2 + Q_{ij,t,\omega}^2 \end{cases} \tag{2}$$

#### *3) SOP Constraints*

Active power can be transferred between different terminals through the SOP, and reactive power can be compensated by the SOP. The SOP operation constraints can be written as:

$$\begin{cases} \left(P_{i,t,\omega}^{\text{SOP}}\right)^2 + \left(Q_{i,t,\omega}^{\text{SOP}}\right)^2 \le \left(S_i^{\text{SOP}}\right)^2 \\ \sum\limits_{i \in \Psi_{\text{nd}}^{\text{SOP}}} P_{i,t,\omega}^{\text{SOP}} + \sum\limits_{i \in \Psi_{\text{nd}}^{\text{SOP}}} P_{i,t,\omega}^{\text{SOP,L}} = 0 \\ P_{i,t,\omega}^{\text{SOP,L}} = A_i^{\text{SOP}} \sqrt{\left(P_{i,t,\omega}^{\text{SOP}}\right)^2 + \left(Q_{i,t,\omega}^{\text{SOP}}\right)^2} \end{cases} \tag{3}$$

#### *4) ESS Constraints*

During one period, active power can only be charged into the ESS or discharged from the ESS. In addition, the SOC of ESS is also constrained.

$$\begin{cases} \gamma_{i,t,\omega}^{\text{dis}} + \gamma_{i,t,\omega}^{\text{ch}} \le 1 \quad \gamma_{i,t,\omega}^{\text{dis}}, \gamma_{i,t,\omega}^{\text{ch}} \in \{0,1\} \\ 0 \le P_{i,t,\omega}^{\text{ch}} \le P_{i,\max}^{\text{ch}} \gamma_{i,t,\omega}^{\text{ch}} \\ 0 \le P_{i,t,\omega}^{\text{dis}} \le P_{i,\max}^{\text{dis}} \gamma_{i,t,\omega}^{\text{dis}} \\ E_{i,\text{ini},\omega} = E_{i,T,\omega} \\ E_{i,t,\omega} = E_{i,t-1,\omega} + \dfrac{\eta_i^{\text{ch}} P_{i,t,\omega}^{\text{ch}} \Delta t}{S_i^{\text{ESS}}} - \dfrac{P_{i,t,\omega}^{\text{dis}} \Delta t}{\eta_i^{\text{dis}} S_i^{\text{ESS}}} \\ E_{\min} \le E_{i,t,\omega} \le E_{\max} \end{cases} \tag{4}$$

*5) SVC Constraints*

The reactive power of the SVC can be adjusted continuously, and the operation constraint of the SVC is expressed as:

$$Q_{i,\min}^{\mathrm{SVC}} \le Q_{i,t,\omega}^{\mathrm{SVC}} \le Q_{i,\max}^{\mathrm{SVC}} \tag{5}$$

*6) SCB Constraints*

Different from the SVC, the reactive power of the SCB is adjusted by switching discrete banks on or off.

$$\begin{cases} Q_{i,t}^{\mathrm{SCB}} = N_{i,t}^{\mathrm{SCB}} q_{\mathrm{SCB}} \\ 0 \le N_{i,t}^{\mathrm{SCB}} \le N_{\max}^{\mathrm{SCB}} \\ \sum_{t=1}^{T} \left| N_{i,t}^{\mathrm{SCB}} - N_{i,t-1}^{\mathrm{SCB}} \right| \le \Delta_{\max}^{\mathrm{SCB}} \end{cases} \tag{6}$$

*7) Security Constraints*

$$\begin{cases} u_{i,\min} \le u_{i,t,\omega} \le u_{i,\max} \\ 0 \le i_{ij,t,\omega} \le i_{ij,\max} \end{cases} \tag{7}$$

The decision variables of P0 are shown in (8).

$$x^{\mathrm{da}} = \left\{ N_{i,t}^{\mathrm{SCB}} \right\} \tag{8}$$

Since optimizing SCB schedules is not the main focus of this paper, algorithm details for solving the model will not be included here. If power flow constraints and SOP constraints are transformed into convex constraints, a mixed-integer second-order cone programming (MISOCP) algorithm can be applied here. The transformation of nonconvex power flow constraints can be reviewed in [16]. Otherwise, a heuristic algorithm such as the particle swarm optimization (PSO) algorithm is another choice.

## B. Equivalent Power Balancing Model Between Networks

*1) Objective Function*

The power balancing model between networks minimizes the total purchased active power from the upstream grid. According to the power flow calculation formulas, the purchased active power equals the sum of net active loads and active power loss in an ADN. Consequently, the objective function in scenario $\omega$ from $\Omega_{\mathrm{sen}}^{\mathrm{sto}}$ is expressed as:

$$\text{(P1)}\ \min f_{\omega}^{\mathrm{da,o}} = \sum_{m=1}^{N} \sum_{t=1}^{T} \left( P_{m,t,\omega}^{\mathrm{nl}} - P_{m,t,\omega}^{\mathrm{SOP}} + \sum_{ij \in \Phi_{\mathrm{br}}^{m}} i_{m,ij,t,\omega} r_{ij,m} \right) \tag{9}$$

*2) Sensitivity Constraints*

To prevent voltage and current violations, the sensitivities of node power to voltage and current are considered. The computation of sensitivities can be reviewed in [24].

The power flow calculation formula of the Newton-Raphson method is shown in (10).

$$\begin{bmatrix} \Delta \boldsymbol{P}_{t,\omega} \\ \Delta \boldsymbol{Q}_{t,\omega} \end{bmatrix} = \begin{bmatrix} \boldsymbol{J}_{t,\omega}^{P\theta} & \boldsymbol{J}_{t,\omega}^{PU} \\ \boldsymbol{J}_{t,\omega}^{Q\theta} & \boldsymbol{J}_{t,\omega}^{QU} \end{bmatrix} \begin{bmatrix} \Delta \boldsymbol{\theta}_{t,\omega} \\ \Delta \boldsymbol{U}_{t,\omega} \end{bmatrix} \quad \omega \in \Omega_{\mathrm{sen}}^{\mathrm{sto}} \tag{10}$$

According to (10), the deviation of node voltage with respect to node power can be written as:

$$\begin{cases} \Delta \boldsymbol{U}_{t,\omega} = \boldsymbol{J}_{1,t,\omega} \left( \Delta \boldsymbol{Q}_{t,\omega} - \boldsymbol{J}_{2,t,\omega} \Delta \boldsymbol{P}_{t,\omega} \right) \\ \boldsymbol{J}_{1,t,\omega} = \left( \boldsymbol{J}_{t,\omega}^{QU} - \boldsymbol{J}_{t,\omega}^{Q\theta} \left( \boldsymbol{J}_{t,\omega}^{P\theta} \right)^{-1} \boldsymbol{J}_{t,\omega}^{PU} \right)^{-1} \\ \boldsymbol{J}_{2,t,\omega} = \boldsymbol{J}_{t,\omega}^{Q\theta} \left( \boldsymbol{J}_{t,\omega}^{P\theta} \right)^{-1} \end{cases} \tag{11}$$

Therefore, the computation of the updated node voltage can be expressed as:

$$\boldsymbol{U}'_{t,\omega} = \boldsymbol{U}_{t,\omega}^{0} - \Delta \boldsymbol{U}_{t,\omega} \tag{12}$$

For the sensitivity of branch current with respect to node active power, the computation formula of branch current can be expressed as:

$$I_{ij,t,\omega} = \sqrt{\frac{U_{i,t,\omega}^2 + U_{j,t,\omega}^2 - 2U_{i,t,\omega} U_{j,t,\omega} \cos \theta_{ij,t,\omega}}{r_{ij}^2 + x_{ij}^2}} \tag{13}$$

According to the full differential formula, the sensitivity of the branch current with respect to the node active power and node reactive power is shown in (14).

$$\begin{cases} \dfrac{\partial I_{ij,t,\omega}}{\partial P_{k,t,\omega}} = \dfrac{\partial I_{ij,t,\omega}}{\partial U_{k,t,\omega}} \dfrac{\partial U_{k,t,\omega}}{\partial P_{k,t,\omega}} + \dfrac{\partial I_{ij,t,\omega}}{\partial \theta_{k,t,\omega}} \dfrac{\partial \theta_{k,t,\omega}}{\partial P_{k,t,\omega}} \\ \dfrac{\partial I_{ij,t,\omega}}{\partial Q_{k,t,\omega}} = \dfrac{\partial I_{ij,t,\omega}}{\partial U_{k,t,\omega}} \dfrac{\partial U_{k,t,\omega}}{\partial Q_{k,t,\omega}} + \dfrac{\partial I_{ij,t,\omega}}{\partial \theta_{k,t,\omega}} \dfrac{\partial \theta_{k,t,\omega}}{\partial Q_{k,t,\omega}} \end{cases} \tag{14}$$

Formula (14) can be transformed into matrix form, which is expressed as:

$$\begin{bmatrix} \boldsymbol{M}_{t,\omega}^{I\theta} \\ \boldsymbol{M}_{t,\omega}^{IU} \end{bmatrix} = \begin{bmatrix} \boldsymbol{J}_{t,\omega}^{P\theta} & \boldsymbol{J}_{t,\omega}^{PU} \\ \boldsymbol{J}_{t,\omega}^{Q\theta} & \boldsymbol{J}_{t,\omega}^{QU} \end{bmatrix} \begin{bmatrix} \boldsymbol{\delta}_{t,\omega}^{IP} \\ \boldsymbol{\delta}_{t,\omega}^{IQ} \end{bmatrix} \tag{15}$$

Therefore, the calculation formula of elements in the sensitivity matrix is shown in (16).

$$\begin{bmatrix} \boldsymbol{\delta}_{t,\omega}^{IP} \\ \boldsymbol{\delta}_{t,\omega}^{IQ} \end{bmatrix} = \left( \boldsymbol{J}^{T} \right)^{-1} \begin{bmatrix} \boldsymbol{M}_{t,\omega}^{I\theta} \\ \boldsymbol{M}_{t,\omega}^{IU} \end{bmatrix} \tag{16}$$

The updated branch current with sensitivity is expressed as:

$$\begin{cases} \boldsymbol{I}'_{t,\omega} = \boldsymbol{I}_{t,\omega}^{0} - \Delta \boldsymbol{I}_{t,\omega} \\ \Delta \boldsymbol{I}_{t,\omega} = \boldsymbol{\delta}_{t,\omega}^{IP} \Delta \boldsymbol{P}_{t,\omega} + \boldsymbol{\delta}_{t,\omega}^{IQ} \Delta \boldsymbol{Q}_{t,\omega} \end{cases} \tag{17}$$

Moreover, the node voltage magnitude and branch current must comply with the security constraint (7).

The decision variables of P1 are shown as:

$$x_{\omega}^{\mathrm{da,o}} = \left\{ P_{i,t,\omega}^{\mathrm{SOP}}, Q_{i,t,\omega}^{\mathrm{SOP}} \right\} \tag{18}$$

*3) ORs of SOP*

In the day-ahead scheduling stage, ORs are composed of ORs in each hour. It should be emphasized that the ORs of the active power of SOP are constraints about its active power, designed for intraday hourly optimization. For period $t$, the whole forecast interval is equally divided into several small intervals. The minimum and maximum values of $P_{i,t,\omega}^{\mathrm{SOP}}$ in each small interval are chosen as the bounds for the OR. An example of the ORs of active power of the SOP can be found in Fig. 2. Formulas of the ORs of active power of SOP are shown as:

$$\begin{cases} P_{i,t,k,\min}^{\mathrm{SOP}} \le P_{i,t,k}^{\mathrm{SOP}} \le P_{i,t,k,\max}^{\mathrm{SOP}} \quad \varepsilon_{\min} + (k-1)\varepsilon_s \le \varepsilon_k < \varepsilon_{\min} + k\varepsilon_s \\ \varepsilon_s = \dfrac{\varepsilon_{\max} - \varepsilon_{\min}}{N^{\mathrm{E}}} \\ 1 \le k \le N^{\mathrm{E}} \\ P_{i,t,k,\min}^{\mathrm{SOP}} = \min\limits_{\omega \in \Xi_k^{\varepsilon}} P_{i,t,\omega}^{\mathrm{SOP}} \\ P_{i,t,k,\max}^{\mathrm{SOP}} = \max\limits_{\omega \in \Xi_k^{\varepsilon}} P_{i,t,\omega}^{\mathrm{SOP}} \end{cases} \tag{19}$$

### C. Power Balancing Model Within Network

#### 1) Objective Function and Constraints

To further obtain the ORs of the SOC of ESS for the subsequent intraday stage, each network has to be optimized separately. For each single network, the power balancing model minimizes the sum of purchased active power and its weighted sum of peak-valley differences, which is shown in (20). The research subject is network $m$ in scenario $\omega$ from $\Omega_{\text{sen}}^{\text{sto}}$.

$$\text{(P2)}\ \min f_{m,\omega}^{\text{da,i}} = \sum_{t=1}^{T} P_{m,t,\omega}^{\text{up}} + \sum_{t_c^1, t_c^2 \in \Theta_c^{\text{up}}} \alpha_{m,c,\omega} \left| P_{m,t_c^1,\omega}^{\text{up}} - P_{m,t_c^2,\omega}^{\text{up}} \right| \tag{20}$$

The hourly purchased active power before optimization, denoted as $P_{m,t,\omega}^{\text{up,b}}$, is sorted in ascending order. Then, by pairing the head and tail active power, 12 pairs are formed. Each pair is weighted from high to low to show that reducing the maximum valley-peak difference is the most important step. The formula of weight is shown in (21).

$$\alpha_{m,c,\omega} = \frac{\left| P_{m,t_c^1,\omega}^{\text{up,b}} - P_{m,t_c^2,\omega}^{\text{up,b}} \right|}{\sum\limits_{t_c^1, t_c^2 \in \Theta_c^{\text{up}}} \left| P_{m,t_c^1,\omega}^{\text{up,b}} - P_{m,t_c^2,\omega}^{\text{up,b}} \right|} \tag{21}$$

To transform the objective to the linear form of decision variables, variable substitutions are made, and related constraints are added, as shown in (23).

$$\min f_{m,\omega}^{\text{da,i}} = \sum_{t=1}^{T} P_{m,t,\omega}^{\text{up}} + \sum_{t_c^1, t_c^2 \in \Theta_c^{\text{up}}} \alpha_{m,c,\omega} \Delta P_{m,\omega,t_c^1,t_c^2}^{\text{up}} \tag{22}$$

s.t.

$$\begin{cases} \Delta P_{m,\omega,t_c^1,t_c^2}^{\text{up}} \ge P_{m,t_c^1,\omega}^{\text{up}} - P_{m,t_c^2,\omega}^{\text{up}} \\ \Delta P_{m,\omega,t_c^1,t_c^2}^{\text{up}} \ge P_{m,t_c^2,\omega}^{\text{up}} - P_{m,t_c^1,\omega}^{\text{up}} \end{cases} \tag{23}$$

Constraints of P2 mainly include (3), (4), (5), and (7). The decision variables of P2 are shown as:

$$x_{\omega}^{\text{da,i}} = \left\{ P_{i,t,\omega}^{\text{ch}}, P_{i,t,\omega}^{\text{dis}}, E_{i,t,\omega} \right\} \tag{24}$$

#### 2) ORs of ESS

Similar to the above steps, we can obtain the ORs of SOC of ESS as:

$$\begin{cases} E_{i,t,k,\min} \le E_{i,t,k} \le E_{i,t,k,\max} \quad \varepsilon_{\min} + (k-1)\varepsilon_s \le \varepsilon_k < \varepsilon_{\min} + k\varepsilon_s \\ \varepsilon_s = \dfrac{\varepsilon_{\max} - \varepsilon_{\min}}{N^E} \\ 1 \le k \le N^E \\ E_{i,t,k,\min} = \min\limits_{\omega \in \Xi_k^e} E_{i,t,\omega} \\ E_{i,t,k,\max} = \max\limits_{\omega \in \Xi_k^e} E_{i,t,\omega} \end{cases} \tag{25}$$

## IV. Power Balancing Model in Intraday Corrective Control Stage

The ORs of the active power of SOP and the SOC of ESS are constructed in the day-ahead scheduling stage, which provides operating bounds for the SOP and ESS in the intraday hourly optimization model.

Generally, day-ahead forecast data are not the same as intraday hourly forecast data. Herein, corrective control must be performed on the power of the SOP and ESS hourly based on day-ahead schedules. Since optimization is carried out hourly during the day, a detailed model can be established. Meanwhile, the objective function minimizes the weighted sum of the hourly purchase cost of electricity from the upstream grid and the voltage deviations.

$$\text{(P3)}\ \min f^{\text{in}} = \alpha_{\text{up}} \sum_{m=1}^{N} \frac{\sum\limits_{t=1}^{T} c_t^{\text{pur}} P_{m,t}^{\text{up}}}{f_m^{\text{up}}} + \alpha_{\text{vd}} \sum_{m=1}^{N} \frac{\sum\limits_{i \in \Psi_{\text{nd}}^m} \sum\limits_{t=1}^{T} \left| u_{i,m,t} - 1 \right|}{f_m^{\text{vd}}} \tag{26}$$

$\alpha_{\text{up}}$ and $\alpha_{\text{vd}}$ are obtained by the analytical hierarchy process (AHP) method. Variable substitution is applied to transform the objective function into a linear form.

$$\min f^{\text{in}} = \alpha_{\text{up}} \sum_{m=1}^{N} \frac{\sum\limits_{t=1}^{T} c_t^{\text{pur}} P_{m,t}^{\text{up}}}{f_m^{\text{up}}} + \alpha_{\text{vd}} \sum_{m=1}^{N} \frac{\sum\limits_{i \in \Psi_{\text{nd}}^m} \sum\limits_{t=1}^{T} u'_{i,m,t}}{f_m^{\text{vd}}} \tag{27}$$

s.t.

$$\begin{cases} u'_{i,m,t} \ge u_{i,m,t} - 1 \\ u'_{i,m,t} \ge 1 - u_{i,m,t} \end{cases} \tag{28}$$

For the intraday model, the constraints of the active power of SOP and the SOC of ESS must be extracted from the ORs. First, the intraday forecast error is calculated and compared with the day-ahead forecast data in period $t$. Then, the small interval that the error locates is determined and denoted as $k_t$. The ranges for $P_{i,t}^{\text{SOP}}$ and $E_{i,t}$ are the constraints, as shown in (29).

$$\begin{cases} P_{i,t,k_t,\min}^{\text{SOP}} \le P_{i,t}^{\text{SOP}} \le P_{i,t,k_t,\max}^{\text{SOP}} \\ E_{i,t,k_t,\min} \le E_{i,t} \le E_{i,t,k_t,\max} \end{cases} \quad 1 \le t \le T \tag{29}$$

Considering the above, other constraints of power flow and regulatory resources in each network are included, which are described in Section III-A. The decision variables of P3 are shown as:

$$x^{\text{in}} = \left\{ P_{i,t,\omega}^{\text{SOP}}, Q_{i,t,\omega}^{\text{SOP}}, P_{i,t,\omega}^{\text{ch}}, P_{i,t,\omega}^{\text{dis}}, E_{i,t,\omega} \right\} \tag{30}$$

## V. Implementation Algorithm

### A. Transformation of Nonconvex Constraints

Conic relaxation is applied to transform the nonconvex constraints of the sixth constraint in (2) and the third constraint in (3). The transformed constraints are shown as:

$$\left\| \left[ 2P_{ij,t,\omega} \quad 2Q_{ij,t,\omega} \quad i_{ij,t,\omega} - u_{i,t,\omega} \right] \right\|_2^{\text{T}} \le i_{ij,t,\omega} + u_{i,t,\omega} \tag{31}$$

$$\left( P_{i,t,\omega}^{\text{SOP}} \right)^2 + \left( Q_{i,t,\omega}^{\text{SOP}} \right)^2 \le \left( \frac{P_{i,t,\omega}^{\text{SOP,L}}}{A_i^{\text{SOP}}} \right)^2 \tag{32}$$

### B. ADMM for Flexibly Interconnected ADNs

Flexibly interconnected ADNs can be partitioned and bounded by the DC side of the SOP. Each independent ADN with the AC side of the SOP comprises one control area. The ADMM blends the decomposability of dual ascent with the superior convergence properties of the method of multipliers, which is applicable here [25].

The active power balance constraint of the SOP should be ensured between different areas. As observed from constraint (3), only boundary active power is exchanged between areas. Taking SOP1 in Fig. 1 as an example, the first constraint in (3) can be rewritten as:

$$\begin{cases} P_{i,t,\omega}^{\mathrm{SOP}}+P_{i,t,\omega}^{\mathrm{SOP,L}}=P^{\mathrm{link}} \\ P_{j,t,\omega}^{\mathrm{SOP}}+P_{j,t,\omega}^{\mathrm{SOP,L}}=-P^{\mathrm{link}} \end{cases} \tag{33}$$

For the flexibly interconnected ADN in Fig. 1, the objective function for the spatial power balance in the day-ahead stage can be expressed as:

$$\begin{cases} \min f_{\omega}^{\mathrm{da,o}}=f_1+f_2 \\ f_1=P_{1,t,\omega}^{\mathrm{nl}}-P_{1,t,\omega}^{\mathrm{SOP}}+\sum\limits_{ij\in\Phi_{\mathrm{br}}^{1}} i_{1,ij,t,\omega}r_{ij,1} \\ f_2=P_{2,t,\omega}^{\mathrm{nl}}-P_{2,t,\omega}^{\mathrm{SOP}}+\sum\limits_{ij\in\Phi_{\mathrm{br}}^{2}} i_{2,ij,t,\omega}r_{ij,2} \end{cases} \tag{34}$$

Taking Network 1 in Fig. 1 as an example, let $\lambda$ denote the Lagrange multiplier for the active power balance constraint between areas and $\rho$ denote the penalty factor. Then, the objective function of Network 1 can be rewritten as:

$$L_{\mathrm{NW1}}^{\mathrm{ADMM}}=f_1+\frac{\rho}{2}\left(P_{i,t}^{\mathrm{SOP}}+P_{i,t}^{\mathrm{SOP,L}}-P^{\mathrm{link}}\right)^2+ \lambda\left(P_{i,t}^{\mathrm{SOP}}+P_{i,t}^{\mathrm{SOP,L}}-P^{\mathrm{link}}\right) \tag{35}$$

Operation optimization is carried out for each network. The optimization results of the regulatory devices and boundary active power are obtained. The global value of the boundary data between areas should be updated according to (36).

$$P_{l+1}^{\mathrm{link}}=\frac{P_{i,t,l+1}^{\mathrm{SOP}}+P_{i,t,l+1}^{\mathrm{SOP,L}}-P_{j,t,l+1}^{\mathrm{SOP}}+P_{j,t,l+1}^{\mathrm{SOP,L}}}{2} \tag{36}$$

After obtaining the global value, the computation formulas of the raw residual and the dual residual can be expressed as:

$$\begin{cases} w_1^{l+1}=\left|P_{i,t,l+1}^{\mathrm{SOP}}+P_{i,t,l+1}^{\mathrm{SOP,L}}-P_{l+1}^{\mathrm{link}}\right| \\ s_1^{l+1}=\left|P_{l+1}^{\mathrm{link}}-P_{l}^{\mathrm{link}}\right| \end{cases} \tag{37}$$

Then, based on the boundary active power, the Lagrange multiplier should be updated as:

$$\lambda_{l+1}=\lambda_l+\rho\left(P_{l+1}^{\mathrm{link}}-P_{i,t,l+1}^{\mathrm{SOP}}-P_{i,t,l+1}^{\mathrm{SOP,L}}\right) \tag{38}$$

The detailed process of the distributed coordination optimization for flexibly interconnected ADNs with SOPs is summarized below.

*Step 1*: initialization. The power flow results of the network without regulatory devices are set as initial values. Then, obtain $P_0^{\mathrm{link}}$ based on the initial values. Set the initial Lagrange multiplier as 0 and $l=0$.

*Step 2*: optimization. Power flow optimization is carried out for each network, and decision variables and interactive variables are obtained.

*Step 3*: update. Update the global value according to (36). Then, the corresponding Lagrange multiplier is updated according to (38).

*Step 4*: iteration. Obtain the raw residual and the dual residual of each network according to (37). If the infinite norm of the residual is less than the convergence threshold, stop the iteration and output optimal results. Otherwise, let $l=l+1$ and return to *Step 2*.

Following the details mentioned above, the implementation process of the proposed two-stage optimization strategy for spatiotemporal power balancing in flexibly interconnected ADNs is summarized in Algorithm 1, where the day-ahead scheduling stage is shown in lines 2-8, the intraday corrective control stage is shown in lines 9-16, and the problem transformations are shown in lines 15-17.

**Algorithm 1**

1: **Input**: parameters of networks and devices and forecast data
2: Generate large numbers of stochastic scenarios $\Omega_{\mathrm{sen}}^{\mathrm{sto}}$ based on day-ahead forecast data of WT through Monte Carlo method
3: Generate several typical scenarios $\Omega_{\mathrm{sen}}^{\mathrm{typ}}$ through *K*-means cluster algorithm
4: Formulate the model to determine schedules for SCB as P0 (1) and solve it
5: Formulate the equivalent day-ahead spatial power balancing model between networks and approximate it as P1 (9) via problem transformations (lines 15-17)
6: Obtain the ORs of the active power of SOP with the forecast error in each hour
7: Formulate the day-ahead temporal power balancing model within the network and approximate it as P2 (20) via problem transformations for each network
8: Obtain ORs of the SOC of ESS with the forecast error in each hour
9: **for** $t=1$:$T$ **do**
10: Collect hourly forecast data of WT
11: Extract the ORs of the active power of SOP and the SOC of ESS according to the hourly forecast error of WT
12: Formulate the intraday corrective control model
13: Execute problem transformations for P3 (26)
14: Solve the above problem via ADMM and the power of SOP, ESS, and SVC is finally determined
15: $t:=t+1$
16: **end for**
17: Linearize the objective function through variable substitution
18: Transform nonconvex constraints into second-order conic constraints
19: P1 and P3 are reformulated as second-order cone programming (SOCP) problems, while P2 is reformulated as an MISOCP problem
20: **Output**: hourly scheduling strategies for SOPs, ESSs, SVCs, and SCBs

## VI. Case Study

### A. Simulation Setups

The case shown in Fig. 1 is denoted as Case 1. The load curves in the two networks are set to be different, while the WT power curves are the same. The normalized load curves and day-ahead and intraday hourly forecast active power of the WT are depicted in Fig. 3. The day-ahead forecast error $\varepsilon$ for WT is set to be ±20%. The day-ahead hourly forecast data are considered to conform to a uniform distribution within the error range. The parameters for integrated devices are shown in Table I. The parameter settings are shown in Table II.

In Table I, $S$ denotes the capacity of each device. The proposed model was implemented in MATLAB R2017b scripts and solved with CPLEX 12.8. The numerical experiments were performed on a PC with an Intel CPU i5-8300h and 16 GB of RAM.

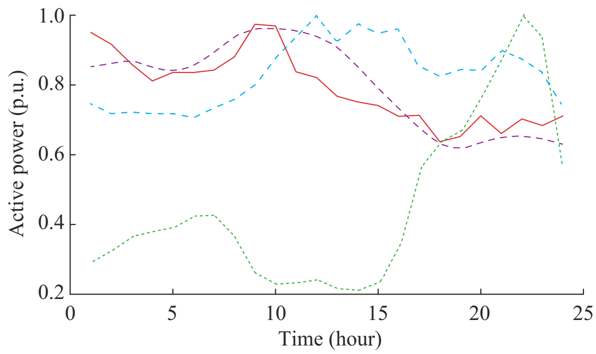


Fig. 3. Normalized load curves and day-ahead and intraday hourly forecast active power of WT.

TABLE I
PARAMETERS FOR INTEGRATED DEVICES

| Device | Location | Parameter |
|---|---|---|
| WT | Nodes 10 and 25 in Network 1 and Node 15 in Network 2 | $S^{WT}=500$ kW |
| ESS | Node 15 in Network 1 and Node 33 in Network 2 | $S^{ESS}=800$ kWh, $P^{ESS,C}_{max}=P^{ESS,D}_{max}=200$ kW/h, $\eta^C=\eta^D=0.9$, $E_{min}=0.2$, $E_{max}=0.9$ |
| SVC | Node 33 in Network 1 and Node 9 in Network 2 | $S^{SVC}=500$ kvar |
| SOP | Node 30 in Network 1 and Node 18 in Network 2 | $S^{SOP}=2$ MVA, $A^{SOP}=0.02$ |
| SCB | Node 8 in Network 1 and Node 29 in Network 2 | $q^{SCB}=100$ kvar, $N^{SCB}_{max}=10$, $\Delta^{SCB}_{max}=3$ |

TABLE II
PARAMETER SETTINGS

| Parameter | Value |
|---|---|
| $c_t^{pur}$ | 01:00-07:00: 61 \$/MWh; 08:00-10:00, 16:00-18:00, 22:00-23:00: 138 \$/MWh; 09:00-15:00, 19:00-21:00: 220 \$/MWh |
| $U_{min}$, $U_{max}$ | 0.93 p.u., 1.07 p.u. |

## *B. Result Analysis for Day-ahead Equivalent Model Considering Sensitivity*

### *1) Error Analysis for Equivalent Model Considering Sensitivity*

To analyze the errors of optimization results such as node voltage and branch current, power flow calculation is carried out after the optimization based on the active power of SOP obtained from the equivalent model. Consequently, the average errors and maximum errors of the node voltage and branch current are shown in Table III.

In Table III, we can observe that the maximum errors are less than 0.1, respectively, which is acceptable. In addition, the average errors of node voltage and branch current are at the $10^{-4}$ and $10^{-3}$ levels, which indicates that the proposed equivalent model is highly accurate. It is also verified that none of the scenarios violate the voltage or current limit, which proves that the equivalent model is sufficiently reliable.

TABLE III
ERRORS OF NODE VOLTAGE AND BRANCH CURRENT

| Parameter | Average error | | Maximum error | |
|---|---|---|---|---|
| | Network 1 | Network 2 | Network 1 | Network 2 |
| Node voltage | 0.000600 | 0.009000 | 0.01196 | 0.01966 |
| Branch current | 0.003582 | 0.006195 | 0.04219 | 0.09042 |

### *2) Analysis of Security Constraint Violations*

To verify the superiority of the adoption of sensitivities, an equivalent model without sensitivity-based security constraints is considered as a comparison. Two models with and without consideration of sensitivity are denoted as Model A and Model N, respectively. The results of the violation percent of different scenarios are shown in Table IV. It shows that although branch current violations do not occur in Model N, node voltages in all scenarios exceed the limits. The results indicate that the adoption of sensitivity-constrained node voltage and branch current in the equivalent model is necessary.

TABLE IV
VIOLATION PERCENT OF DIFFERENT SCENARIOS

| Parameter | Violation percent of model A (%) | | Violation percent of model N (%) | |
|---|---|---|---|---|
| | Network 1 | Network 2 | Network 1 | Network 2 |
| Node voltage | 0 | 0 | 0 | 100 |
| Branch current | 0 | 0 | 0 | 0 |

### *3) Comparison with Detailed Model*

In this part, another day-ahead scheduling model between networks is established considering detailed power flow constraints (denoted as detailed model). The ADMM is used to solve the detailed model. The results show that the average computation time in 1000 scenarios using the equivalent model is 1.24 s, while the average computation time in 100 scenarios using the detailed model is 14 s. More than 24 hours are consumed if 1000 scenarios are optimized using the detailed model, which is unacceptable even in the day-ahead scheduling stage. Combined with the analysis of errors, it can be concluded that the equivalent model considering sensitivities computes faster with acceptable accuracy.

## *C. Result Analysis of ORs*

### *1) Intraday Optimization Results Under Different Conditions*

Different conditions are set to compare the optimization results and ORs in different scenarios and error intervals. Six numbers are set for $N^S$, which are 200, 500, 1000, 1500, 2000, and 3000, while four numbers are set for $N^E$, which are $N^S/2$, $N^S/20$, $N^S/50$, and $N^S/100$. In sum, 24 conditions are composed from all combinations. The contours of total costs and voltage deviations in the intraday stage under 24 conditions are shown in Figs. 4 and 5, respectively.

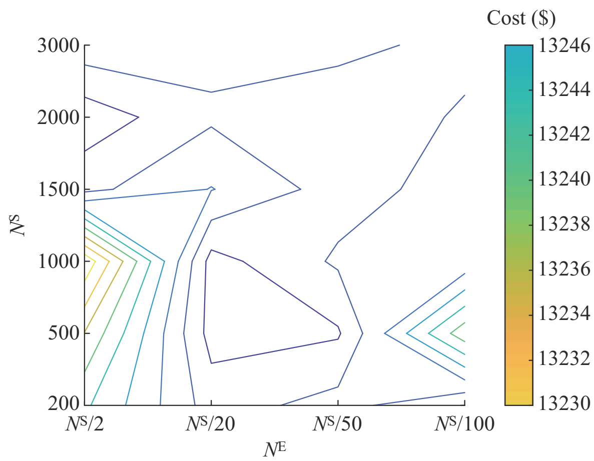


Fig. 4. Contours of total cost under 24 conditions.

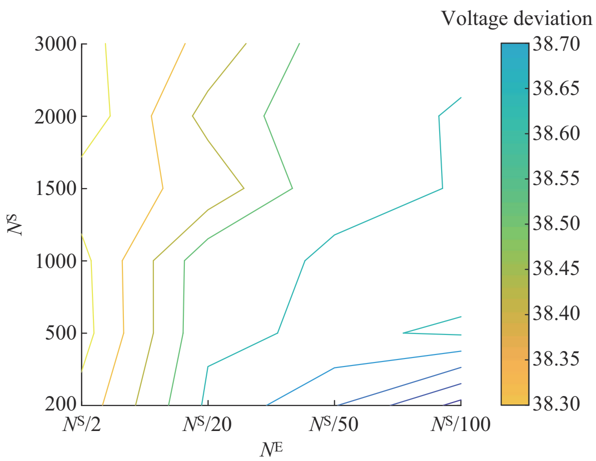


Fig. 5. Contours of voltage deviations under 24 conditions.

In Fig. 4, we can observe that all results are close to each other. There are two valleys, where one valley is for $N^S=2000$ and $N^E=N^S/2$ and the other is composed of data for $N^S=200$, $N^E=N^S/20$, $N^E=N^S/50$ and $N^S=1000$, $N^E=N^S/20$. Figure 4 indicates that cost will not decrease with more $N^S$ and more $N^E$. In Fig. 5, we can also observe that all results are similar. With a smaller $N^S$ and a smaller $N^E$, the voltage deviations are smaller.

*2) ORs Under Different Conditions*

The OR of the active power of SOP in period 19 when $N^S=1500$ and $N^E=N^S/2$ is shown in Fig. 6. Taking ESS1 as an example, the OR of the SOC of ESS1 in period 15 when $N^S=1500$ and $N^E=N^S/2$ is shown in Fig. 7. The orange parts in the two figures are the final ORs in this period according to the intraday hourly forecast error. Combined with ORs in other periods, the final intraday ORs in the time series are obtained, of which examples are shown in Figs. 8 and 9.

The lower and upper bounds of ORs of the active power of SOP in different numbers of scenarios when $N^E=N^S/50$ are shown in Fig. 8(a) and (b), respectively. The lower and upper bounds of ORs of the active power of SOP under different numbers of error intervals when $N^S=2000$ are shown in Fig. 8(c) and (d), respectively. Similar to Fig. 8, the lower and upper bounds of ORs of the SOC of ESS under different numbers of scenarios when $N^E=N^S/20$ are shown in Fig. 9(a) and (b), respectively. The lower and upper bounds of ORs of the SOC of ESS under different numbers of error intervals when $N^S=1000$ are shown in Fig. 9 (c) and (d), respectively.

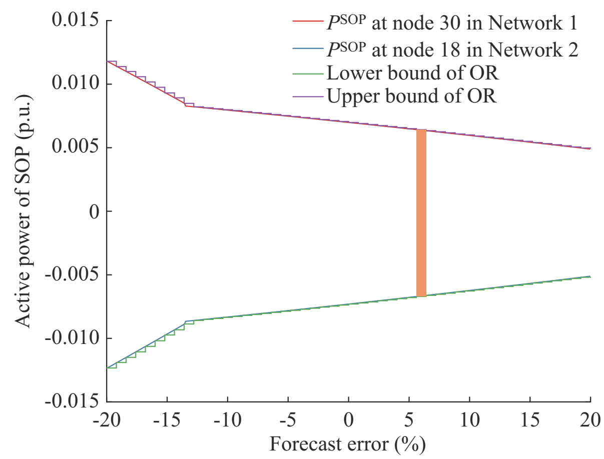


Fig. 6. OR of active power of SOP during period 19 when $N^S=1500$ and $N^E=N^S/2$.

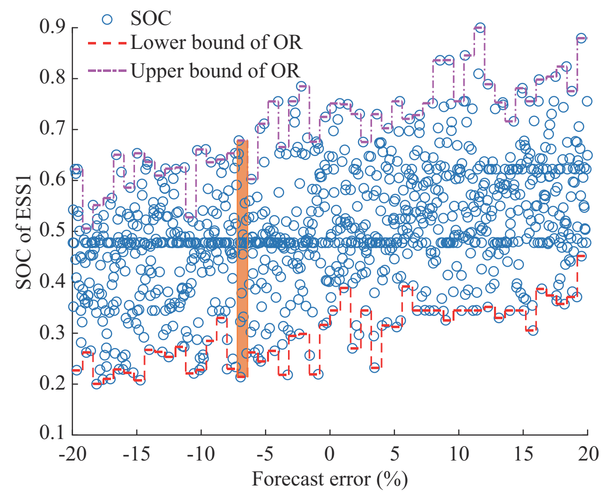


Fig. 7. OR of SOC of ESS1 during period 15 when $N^S=1500$ and $N^E=N^S/2$.

In Fig. 8(a) and (b), we can observe that when $N^S/N^E$ is constant, in more scenarios, the lower bound of the OR increases while the upper bound decreases. This is because the scale of the optimization results becomes larger with more scenarios. Then, with higher data density, it is more likely that smaller or larger values are included and bounds become narrower. Conditions and explanations are also applied to Fig. 9(a) and (b). With more scenarios, the gaps between ORs in different scenarios are smaller.

However, the computation time for the generation of ORs remarkably increases with an increasing number of scenarios. In the day-ahead scheduling stage, the computation time for six scenarios is 2008 s, 7051 s, 11345 s, 15688 s, 20035 s, and 28723 s, respectively.

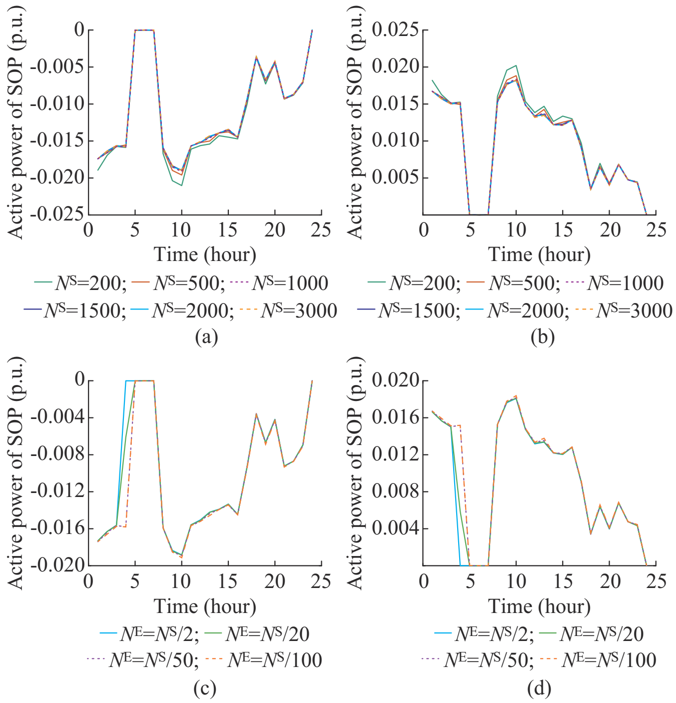


Fig. 8. Lower and upper bounds of ORs of active power of SOP under different $N^S$ or $N^E$. (a) Lower bounds of ORs of active power of SOP under different $N^S$ with $N^E = N^S/50$. (b) Upper bounds of ORs of active power of SOP under different $N^S$ with $N^E = N^S/50$. (c) Lower bounds of ORs of active power of SOP under different $N^E$ with $N^S = 2000$. (d) Upper bounds of ORs of active power of SOP under different $N^E$ with $N^S = 2000$.

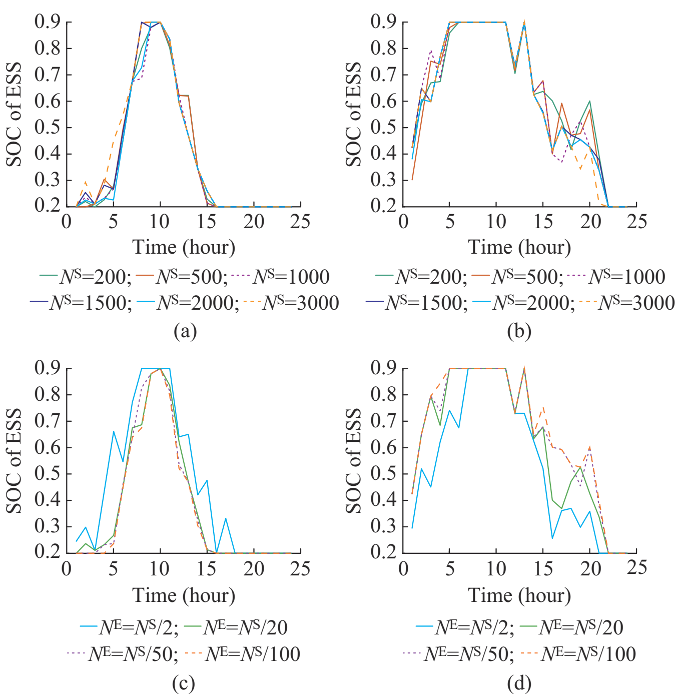


Fig. 9. Lower and upper bounds of ORs of SOC of ESS under different $N^S$ or $N^E$. (a) Lower bounds of ORs of SOC of ESS under different $N^S$ with $N^E = N^S/20$. (b) Upper bounds of ORs of SOC of ESS under different $N^S$ with $N^E = N^S/20$. (c) Lower bounds of ORs of SOC of ESS under different $N^E$ with $N^S = 1000$. (d) Upper bounds of ORs of SOC of ESS under different $N^E$ with $N^S = 1000$.

Figure 8(c) and (d) shows that when $N^S$ is constant, the lower bounds gradually decrease and the upper bounds increase with smaller $N^E$, which also applies to Fig. 9(c) and (d).

Considering the above analysis, it would be suitable to set $N^S = 1500$ and $N^E = N^S/2$.

### 3) *Comparison of Different Schemes*

The ORs of the active power of SOP and the SOC of ESS compose a whole, which means that comparisons cannot be implemented on only one aspect. Consequently, four different schemes for the day-ahead scheduling stage are set to demonstrate the advantages of the ORs. The intraday models for each scheme are the same.

Scheme 1: deterministic day-ahead scheduling model without considering the uncertainty of WT power.

Scheme 2: stochastic day-ahead scheduling model considering the uncertainty of WT power.

Scheme 3: robust day-ahead scheduling model considering the uncertainty of WT power.

Scheme 4: the proposed day-ahead planning model considering sensitivities and the uncertainty of WT power.

In Scheme 4, $N^S = 1500$ and $N^E = N^S/2$. Additionally, regulation strategies for the SCB and ESS are planned day-ahead and irrevocable during the day in Schemes 1, 2, and 3. Comparison of intraday optimization results under different schemes is shown in Table V. The SOP applied in Case 1 consists of two VSCs. For simplicity, the active power of only one terminal, i.e., 1-30, under four schemes is shown in Fig. 10. Taking ESS1 as an example, the corresponding SOCs under four schemes are shown in Fig. 11.

TABLE V
COMPARISON OF INTRADAY OPTIMIZATION RESULTS

| Scheme | Purchase cost of electricity ($) | | | Voltage deviation | | |
|---|---|---|---|---|---|---|
| | Network 1 | Network 2 | Sum | Network 1 | Network 2 | Sum |
| Before optimization | 8637 | 4625 | 13262 | 52.816 | 24.099 | 76.915 |
| 1 | 12308 | 2567 | 14875 | 51.312 | 11.287 | 62.599 |
| 2 | 12410 | 2706 | 15116 | 50.900 | 12.595 | 63.495 |
| 3 | 12410 | 2723 | 15133 | 52.609 | 11.766 | 64.375 |
| 4 | 8212 | 5019 | 13231 | 25.005 | 13.668 | 38.673 |

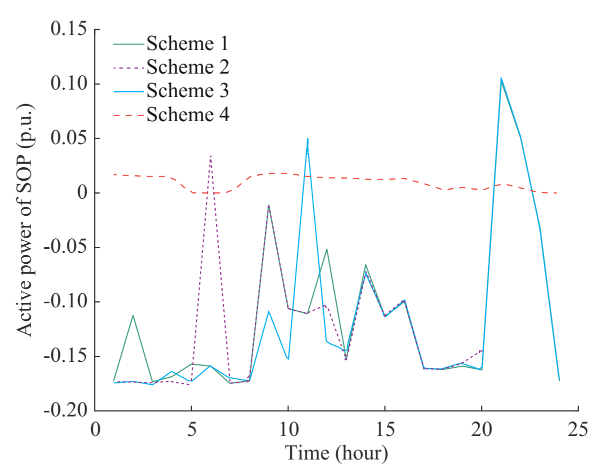


Fig. 10. Active power of SOP under four schemes.

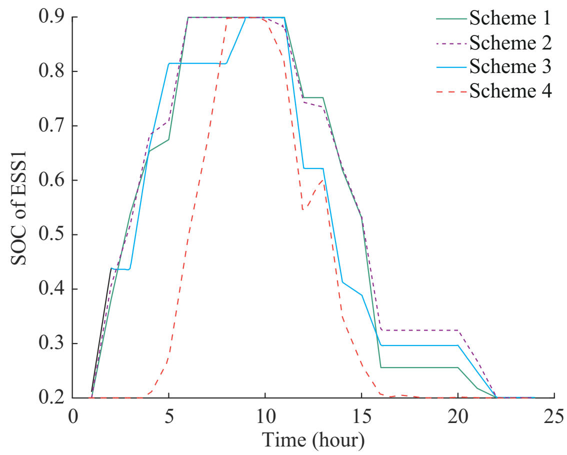


Fig. 11. SOC of ESS1 under four schemes.

Table V shows that the purchase cost of electricity from the upstream grid only decreases under Scheme 4. Combined with the active power of SOP in Fig. 10, different from the other three schemes, active power is transferred from Network 1 to Network 2 due to the limitations of ORs, which indicates that intraday operation economy can be improved by day-ahead power balancing. The cost of Scheme 1 is the lowest of Schemes 1-3. However, the application of Scheme 1 is limited because forecast error is not considered. The cost of Scheme 3 is the highest due to the inclusion of the worst scenario in the robust optimization. Furthermore, we can observe that the voltage deviation of Scheme 4 is far smaller than that of the other schemes in Table V, indicating the superiority of the ORs.

As observed in Fig. 10, curves of the active power of SOP are similar in Schemes 1-3, and more active power is transferred than that in Scheme 4.

Figure 11 shows that the overall trends of the four schemes are similar. Specifically, the rising stages of Schemes 1-3 are similar, while the descending stages of Schemes 1 and 2 are similar. As ESS1 is installed in Network 1, combined with Fig. 3, it can be inferred that ESS1 is charged during the valley-load periods while discharged during the peak-load periods. In addition, considering the unit purchase cost of electricity in Table II, when the unit purchase cost of electricity is low, active power is charged into ESS, and when the unit purchase cost of electricity is high, active power is discharged from ESS, which decreases the total intraday operation cost.

## *D. Algorithm Evaluation*

### *1) Test on a Large System*

Case 2 is based on a demonstration project of SOP in Hangzhou, China. A three-terminal SOP connects three networks, which comprise the 105-node system shown in Fig. 12. The ESS capacity is 1 MWh, and the maximum charging/discharging power is 300 kW. Other ESS parameters and other devices are the same as those in Case 1, as shown in Tables I and II. The day-ahead and intraday hourly forecast active power of the WT and the active loads of the three networks are shown in Fig. 13.

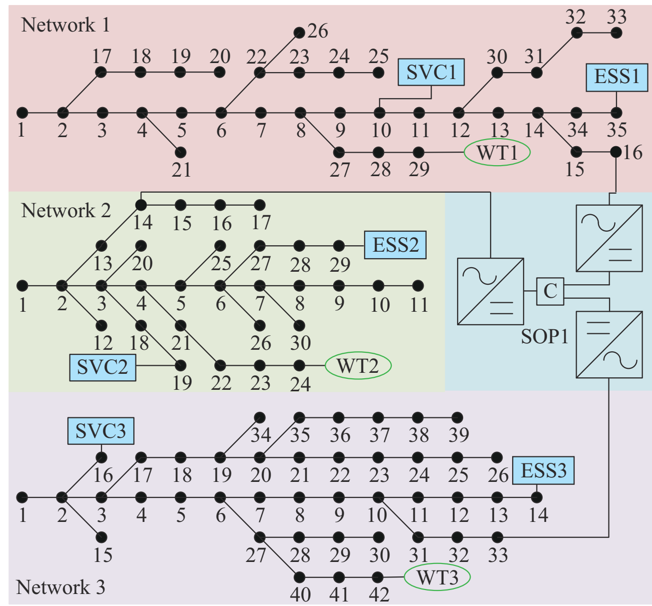


Fig. 12. 105-node system composed of three networks.

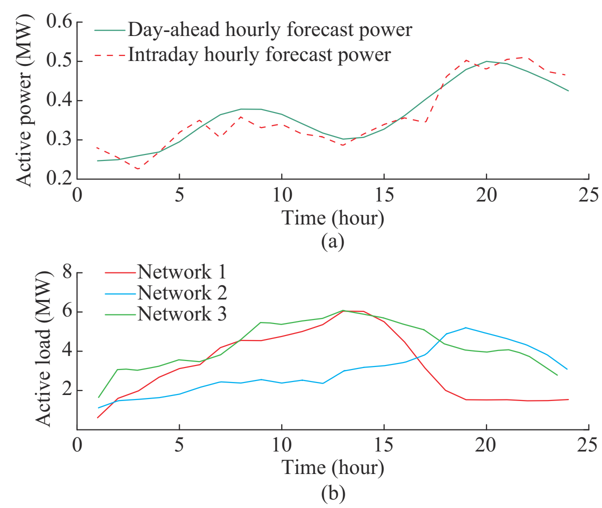


Fig. 13. Day-ahead and intraday hourly forecast active power of WT and active loads of three networks. (a) Day-ahead and intraday hourly forecast power of WT. (b) Active loads of three networks.

In the day-ahead scheduling stage, the maximum voltage and current errors of the equivalent model considering sensitivities are shown in Fig. 14. We can observe that the voltage error during each period is very small, while the current error seems larger but still less than 0.1. Furthermore, voltage or current violations never occur in all stochastic scenarios.

The purchase costs of electricity from the upstream grid and the voltage deviations of the three networks are depicted in Figs. 15 and 16, respectively. In Fig. 15 and Fig. 16, we can observe that the Scheme 4 performs better than the other three schemes. From the above test results and analysis, we can conclude that the proposed optimization strategy for spatiotemporal power balancing considering ORs of the active power of SOPs and the SOC of ESSs exhibits a good scalability performance in applications on larger systems.

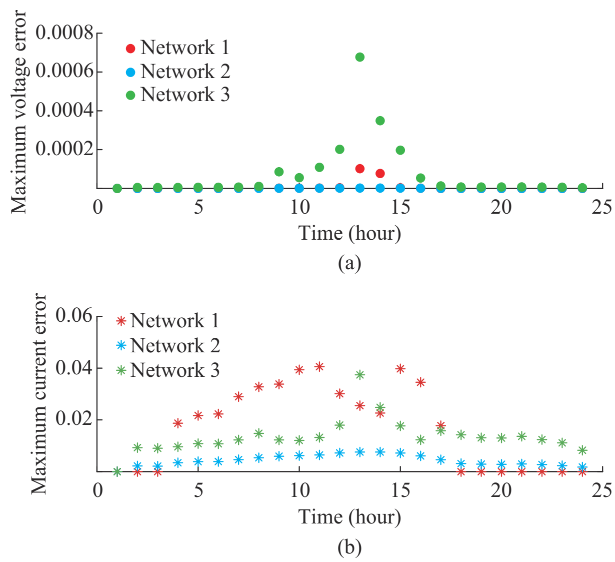


Fig. 14. Maximum voltage and current errors of equivalent model considering sensitivities in day-ahead scheduling stage. (a) Maximum voltage errors. (b) Maximum current errors.

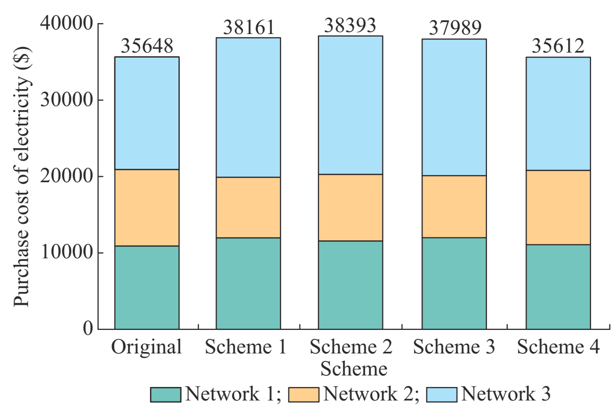


Fig. 15. Purchase cost of electricity from upstream grid of three networks.

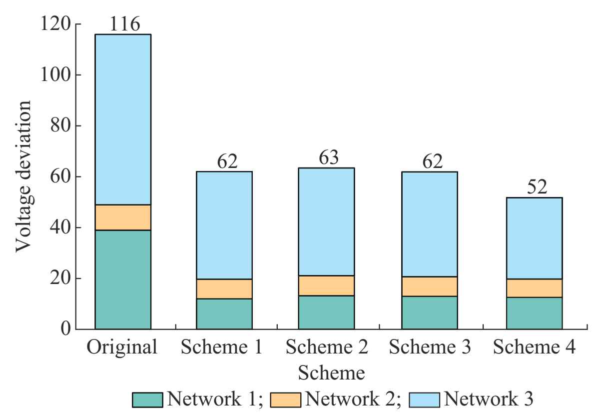


Fig. 16. Voltage deviations of three networks.

### 2) Computation Efficiency

The complexities and computation time of three models, i.e., day-ahead model between networks (P1), day-ahead model within a single network (P2), and intraday corrective control model (P3), are summarized in Table VI to demonstrate the computation performance of the proposed strategy.

TABLE VI
COMPLEXITIES AND COMPUTATION TIME OF THREE MODELS

| Case | Model complexity | | | | | | Computation time (s) | | |
|---|---|---|---|---|---|---|---|---|---|
| | Number of constraints | | | Number of variables | | | | | |
| | P1 | P2 | P3 | P1 | P2 | P3 | P1 | P2 | P3 |
| 1 | 9792 | 31774 | 1481 | 3600 | 15864 | 744 | 1.24 | 9.89 | 5.42 |
| 2 | 15840 | 51924 | 2396 | 5784 | 25926 | 1060 | 2.35 | 12.52 | 10.38 |

Specifically, the number of constraints and variables in the day-ahead scheduling stage corresponds to each stochastic scenario, while that in the intraday corrective control stage corresponds to each hour. Additionally, the computation time for day-ahead models is the average value in 1000 scenarios, while the computation time for the intraday model is the average value in 24 hours.

In Table VI, the computation time for the day-ahead model within the network is obviously more than that between networks because the former is a detailed model with power flow constraints. Meanwhile, the computation time for the intraday corrective control model is far less than 1 hour, which means that the obtained intraday strategy can be easily implemented in the hourly regulation.

## VII. CONCLUSION

In this paper, a two-stage optimization strategy for spatio-temporal power balancing in flexibly interconnected ADNs is proposed. In the day-ahead scheduling stage, considering the uncertainty of WT power, stochastic optimization is carried out to obtain schedules for an SCB with typical scenarios. Then, the ORs of the active power of SOP and the SOC of ESS are obtained from the optimization results in large numbers of stochastic scenarios. To improve computation efficiency, an equivalent model between networks is established, which suppresses violations of system security constraints with sensitivities. In the intraday corrective control stage, different from the existing fixed schedule of ESS regulation, the hourly charging/discharging power of the ESS is flexibly regulated with ORs. The test results reveal that the proposed equivalent model considering sensitivities computes faster than the detailed model, and its error is also acceptable. The power flow calculation result considering the active power of SOP after the optimization proves that voltage or current violations indeed never occur. Meanwhile, the intraday model considering ORs performs better than stochastic optimization and robust optimization, which indicates the superiority of the proposed strategy. For further work, uncertainties in photovoltaic power and loads will be considered. In addition, different settings for the location and capacity of the SOP may affect the power balancing, which is another research topic.

## REFERENCES

[1] P. Li, H. Ji, C. Wang *et al.*, "Coordinated control method of voltage and reactive power for active distribution networks based on soft open point," *IEEE Transactions on Sustainable Energy*, vol. 8, no. 4, pp. 1430-1442, Oct. 2017.
[2] Z. Liu and J. V. Milanović, "Probabilistic estimation of voltage unbal-

ance in MV distribution networks with unbalanced load," *IEEE Transactions on Power Delivery*, vol. 30, no. 2, pp. 693-703, Apr. 2015.

[3] J. M. Bloemink and T. C. Green, "Increasing distributed generation penetration using soft normally-open points," in *Proceedings of IEEE PES General Meeting*, Minneapolis, USA, Aug. 2010, pp. 1-8.

[4] D. Feng, F. Wu, Y. Zhou *et al*., "Multi-agent-based rolling optimization method for restoration scheduling of distribution systems with distributed generation," *Journal of Modern Power Systems and Clean Energy*, vol. 8, no. 4, pp. 737-749, Jul. 2020.

[5] F. Sun, J. Ma, M. Yu *et al*., "Optimized two-time scale robust dispatching method for the multi-terminal soft open point in imbalanced active distribution networks," *IEEE Transactions on Sustainable Energy*, vol. 12, no. 1, pp. 587-598, Jan. 2021.

[6] X. Yang, C. Xu, Y. Zhang *et al*., "Real-time coordinated scheduling for ADNs with soft open points and charging stations," *IEEE Transactions on Power Systems*, vol. 36, no. 6, pp. 5486-5499, Nov. 2021.

[7] H. Ji, C. Wang, P. Li *et al*., "An enhanced SOCP-based method for feeder load balancing using the multi-terminal soft open point in active distribution networks," *Applied Energy*, vol. 208, pp. 986-995, Dec. 2017.

[8] H. Ji, C. Wang, P. Li *et al*., "Robust operation of soft open points in active distribution networks with high penetration of photovoltaic integration," *IEEE Transactions on Sustainable Energy*, vol. 10, no. 1, pp. 280-289, Jan. 2019.

[9] J. Wang, N. Zhou, C. Y. Chung *et al*., "Coordinated planning of converter-based DG units and soft open points incorporating active management in unbalanced distribution networks," *IEEE Transactions on Sustainable Energy*, vol. 11, no. 3, pp. 2015-2027, Jul. 2020.

[10] W. Cao, J. Wu, and N. Jenkins, "Feeder load balancing in MV distribution networks," in *Proceedings of the 2014 IEEE PES Innovative Smart Grid Technologies Europe (ISGT Europe)*, Istanbul, Turkey, Jan. 2014, pp. 1-6.

[11] Z. Ziadi, S. Taira, M. Oshiro *et al*., "Optimal power scheduling for smart grids considering controllable loads and high penetration of photovoltaic generation," *IEEE Transactions on Smart Grid*, vol. 5, no. 5, pp. 2350-2359, Sept. 2014.

[12] Y. J. Kim, J. L. Kirtley, and L. K. Norford, "Reactive power ancillary service of synchronous DGs in coordination with voltage control devices," *IEEE Transactions Smart Grid*, vol. 8, no. 2, pp. 515-527, Mar. 2017.

[13] R. Zafar, J. Ravishankar, J. E. Fletcher *et al*., "Multi-timescale model predictive control of battery energy storage system using conic relaxation in smart distribution grids," *IEEE Transactions on Power Systems*, vol. 33, no. 6, pp. 7152-7161, Nov. 2018.

[14] F. Sun, M. Yu, Q. Wu *et al*., "A multi-time scale energy management method for active distribution networks with multiple terminal soft open point," *International Journal of Electrical Power and Energy Systems*, vol. 128, p. 106767, Jun. 2021.

[15] S. Xie, Z. Hu, and J. Wang, "Two-stage robust optimization for expansion planning of active distribution systems coupled with urban transportation networks," *Applied Energy*, vol. 261, p. 114412, Mar. 2020.

[16] P. Li, Q. Wu, M. Yang *et al*., "Distributed distributionally robust dispatch for integrated transmission-distribution systems," *IEEE Transactions on Power Systems*, vol. 36, no. 2, pp. 1193-1205, Mar. 2021.

[17] S. Talari, M. Yazdaninejad, and M.-R. Haghifam, "Stochastic-based scheduling of the microgrid operation including wind turbines, photovoltaic cells, energy storages and responsive loads," *IET Generation, Transmission & Distribution*, vol. 9, no. 12, pp. 1498-1509, Dec. 2015.

[18] Y. P. Agalgaonkar, B. C. Pal, and R. A. Jabr, "Stochastic distribution system operation considering voltage regulation risks in the presence of PV generation," *IEEE Transactions on Sustainable Energy*, vol. 6, no. 4, pp. 1315-1324, Oct. 2015.

[19] A. X. Sun, D. T. Phan, and S. Ghosh, "Fully decentralized AC optimal power flow algorithms," in *Proceedings of 2013 IEEE PES General Meeting*, Vancouver, Canada, Jan. 2013, pp. 1-5.

[20] W. Zheng, W. Wu, B. Zhang *et al*., "A fully distributed reactive power optimization and control method for active distribution networks," *IEEE Transactions on Smart Grid*, vol. 7, no. 2, pp. 1021-1033, Mar. 2016.

[21] K. Christakou, J. LeBoudec, M. Paolone *et al*., "Efficient computation of sensitivity coefficients of node voltages and line currents in unbalanced radial electrical distribution networks," *IEEE Transactions on Smart Grid*, vol. 4, no. 2, pp. 741-750, Jun. 2013.

[22] G. Valverde and T. van Cutsem, "Model predictive control of voltages in active distribution networks," *IEEE Transactions on Smart Grid*, vol. 4, no. 4, pp. 2152-2161, Dec. 2013.

[23] Y. Guo, Q. Wu, H. Gao *et al*., "Double-time-scale coordinated voltage control in active distribution networks based on MPC," *IEEE Transactions on Sustainable Energy*, vol. 11, no. 1, pp. 294-303, Jan. 2020.

[24] K. Christakou, M. Paolone, and A. Abur, "Voltage control in active distribution networks under uncertainty in the system model: a robust optimization approach," *IEEE Transactions on Smart Grid*, vol. 9, no. 6, pp. 5631-5642, Nov. 2018.

[25] S. Boyd, N. Parikh, E. Chu *et al*., "Distributed optimization and statistical learning via the alternating direction method of multipliers," *Foundations and Trends in Machine Learning*, vol. 3, no. 1, pp. 1-122, Jan. 2011.

**Can Wang** received the B.Eng. degree in electrical engineering and automation from Jilin University, Changchun, China, in 2018. He is currently working toward the Ph.D. degree with the School of Electrical Engineering and Automation, Wuhan University, Wuhan, China. His research interests include operation optimization and planning of active distribution networks.

**Jianjun Sun** received the B.Eng., M.Eng., and Ph.D. degrees in electrical engineering from Wuhan University, Wuhan, China, in 1997, 2000, and 2007, respectively. He is currently a Professor and the Deputy Director of the Motor and Power Electronics Center, School of Electrical Engineering and Automation, Wuhan University, Wuhan, China. His current research interests include multi-layer design of smart grid and of power quality analysis.

**Meng Huang** received the B.Eng. and M.Eng. degrees from the Huazhong University of Science and Technology, Wuhan, China, in 2006 and 2008, respectively, and the Ph.D. degree from Hong Kong Polytechnic University, Hong Kong, China, in 2013. He is currently an Associate Professor with the School of Electrical Engineering and Automation, Wuhan University, Wuhan, China. His research interests include nonlinear analysis of power converters and power electronics reliability.

**Xiaoming Zha** received the B.Eng., M.Eng., and Ph.D. degrees in electrical engineering from Wuhan University, Wuhan, China, in 1989, 1992, and 2001, respectively. He was a Postdoctoral Fellow with the University of Alberta, Edmonton, Canada, from 2001 to 2003. He has been a Faculty Member of Wuhan University since 1992, and became a Professor in 2003. His research interests include power electronic converter, application of power electronics in smart grid and renewable energy generation, analysis and control of microgrid, analysis and control of power quality, and frequency control of high-voltage high-power electric motors.

**Wei Hu** received the B.Eng., M.Eng., and Ph.D. degrees in electrical engineering from Wuhan University, Wuhan, China, in 2003, 2006, and 2015, respectively. She is a Senior Engineer with the State Grid Hubei Electric Power Corporation, Wuhan, China. Her research interests include modeling and power quality analysis of microgrid.